Proteomic Analysis of Microtubule-associated Proteins during Macrophage Activation*[S]

Prerna C. Patel‡, Katherine H. Fisher§¶, Eric C. C. Yang‖, Charlotte M. Deane§¶, and Rene E. Harrison‡**

Classical activation of macrophages induces a wide range of signaling and vesicle trafficking events to produce a more aggressive cellular phenotype. The microtubule (MT) cytoskeleton is crucial for the regulation of immune responses. In the current study, we used a large scale proteomics approach to analyze the change in protein composition of the MT-associated protein (MAP) network by macrophage stimulation with the inflammatory cytokine interferon-γ and the endotoxin lipopolysaccharide. Overall the analysis identified 409 proteins that bound directly or indirectly to MTs. Of these, 52 were up-regulated 2-fold or greater and 42 were down-regulated 2-fold or greater after interferon-γ/lipopolysaccharide stimulation. Bioinformatics analysis based on publicly available binary protein interaction data produced a putative interaction network of MAPs in activated macrophages. We confirmed the up-regulation of several MAPs by immunoblotting and immunofluorescence analysis. More detailed analysis of one up-regulated protein revealed a role for HSP90β in stabilization of the MT cytoskeleton during macrophage activation. ***Molecular & Cellular Proteomics 8:2500–2514, 2009.***

Microtubules (MTs)[1] are major structural components of the cytoskeleton that are intricately involved in cell morphology, motility, division, and intracellular organization and transport. The diverse roles of MTs are dependent on the polymer having the capacity to be both dynamic and static in nature. Individual MTs alternate between growing and shrinking by the rapid attachment and detachment of tubulin subunits at their ends (1, 2). Thus, MTs can continually reorganize and undergo cycles of growing, pausing, and shortening. A number of mechanisms exist to regulate this dynamic equilibrium and involve association of proteins with the MT lattice. MT-associated proteins (MAPs), such as MAP4 and tau, stabilize MTs by binding to the wall thus inhibiting MT disassembly (3, 4). Recently MT plus (+) end-binding proteins have been implicated in stabilizing MTs by associating with cortical proteins to tether the MT end to peripheral target sites (5–7). Stabilized MT subsets are biochemically distinct and acquire posttranslational modifications that can be used to differentiate them from dynamic subsets. For example, posttranslational modifications such as glutamylation (8), detyrosination (8, 9), and acetylation (10) occur on MTs that exhibit increased stability. Stabilized MTs have been implicated in MT transport by allowing increased binding of MT motors (11, 12). Numerous other MAPs have been shown to regulate MT form and function including control of MT nucleation and elongation, MT linkage to and movement of organelles, and modulation of MT growth to allow scaffolding of signal transduction events (13).

The extensive MT network provides a large surface area to serve as a platform for the binding of a large number of proteins that is likely heavily influenced by local cellular events and cell type. Traditionally the term MAP referred to proteins that bind directly to tubulin within the MT polymer, and a lot of recent debate and controversy have surrounded the definition of a MAP (14, 15). In this and other reports the definition of MAPs is considered to also include proteins that indirectly or transiently interact with MTs, co-localize with MTs, or influence MT growth dynamics in some way (16). The advent of proteomics has allowed cytoskeleton researchers to resolve the spectrum of MAPs. To date, the MT proteome has been resolved by MS analysis in developmentally important animal and plant models including *Xenopus laevis* egg extracts (17), *Drosophila melanogaster* embryos (18), *Artemia franciscana* embryos (19), *Arabidopsis* suspension cells (20), and complex mammalian tissues such as rat brain (21). The MT proteome has also been described for specialized MT structures including mitotic spindles (22–24), centrosomes (25, 26), and cilia (27, 28).

From the ‡Department of Biological Sciences, University of Toronto Scarborough, 1265 Military Trail, Toronto, Ontario M1C 1A4, Canada, §Department of Statistics, University of Oxford, Oxford OX1 3TG, United Kingdom, ¶Oxford Doctoral Training Centre, University of Oxford, Oxford OX1 3QD, United Kingdom, and ‖Proteomics Core Facility, Sunnybrook Research Institute, Sunnybrook Health Sciences Centre and University of Toronto, Toronto, Ontario M4N 3M5, Canada

Received, April 20, 2009, and in revised form, July 7, 2009

Published, MCP Papers in Press, August 2, 2009, DOI 10.1074/mcp.M900190-MCP200

[1] The abbreviations used are: MT, microtubule; LPS, lipopolysaccharide; IFN-γ, interferon-γ; MAP, MT-associated protein; HSP, heat shock protein; GA, geldanamycin; DMEM, Dulbecco's modified Eagle's medium; FBS, fetal bovine serum; PIPES, 1,4-piperazinediethanesulfonic acid; AMP-PNP, adenosine 5′-(β,γ-imino)triphosphate; TEM, transmission electron microscopy; Ab, antibody; IF, immunofluorescence; BLAST, basic local alignment search tool; IGUP, interferon-γ up-regulated; MHC, major histocompatibility complex.

Macrophages are key regulators of the immune system connecting innate and specific immune responses. Lipopolysaccharide (LPS), an outer membrane component of Gram-negative bacteria, is a potent activator of monocytes and macrophages. LPS triggers the abundant secretion of many cytokines from macrophages including IL-1 (29), IL-6, (30), and tumor necrosis factor-α (31), which together contributes to the pathophysiology of septic shock. IFN-γ is a proinflammatory cytokine produced by the host in response to intracellular pathogens. IFN-γ binds to IFN-γ receptors on macrophages, and IFN-γ signaling induces the production and/or release of cytokines, like IL-1 or tumor necrosis factor-α, which enhance LPS-mediated effects (32). Thus, the synergy between LPS and inflammatory cytokines such as IFN-γ represents an important regulatory mechanism by which the host tackles a significant, ongoing infection before it activates potent effector responses (33). It has been demonstrated that LPS may cause changes in monocyte cytoskeleton and directly influence assembly of isolated MTs (34). Recently we observed that classical activation of murine resident peritoneal or RAW264.7 macrophages with a combination of IFN-γ and LPS induces an increase in stabilized cytoplasmic MTs (5). A significant effort has been made to unravel the importance of stable MTs in cellular processes over the past few years. With respect to macrophage function, stable MTs could potentially function as tracks for vesicle secretion of cytokines and matrix metalloproteinases necessary to effect the enhanced inflammatory response observed in classically activated macrophages. We recently demonstrated that stable MTs are important for cell spreading as well as the binding of large particles in activated macrophages (5). The stabilization of macrophage interphase MTs is uniquely rapid, thus serving as an ideal model for studying MAPs involved in MT modulation in mammalian cells.

The focus of the present study was to identify the MT-associated proteins involved in altering and stabilizing MT structures and also to resolve the spectrum of proteins within the MT proteome of a mammalian cell. To achieve this goal, we used a proteomics approach involving a MAP purification technique based on MT co-sedimentation (35) followed by off-line fractionation and identification of MAPs using LC-MS/MS. Information provided by mass spectrometry analysis allowed us to analyze the changes in MAP abundance during activation of macrophages by IFN-γ/LPS. These studies also provided candidate proteins for selective molecular intervention for chronic inflammatory disorders.

EXPERIMENTAL PROCEDURES

Reagents and Antibodies—Dulbecco's modified Eagle's medium (DMEM) and fetal bovine serum (FBS) were purchased from Wisent Inc. (Quebec, Canada). Antibodies were obtained as follows. Mouse monoclonal anti-talin, anti-actin, and anti-α-tubulin; anti-dynein; and anti-MAP1 were from Sigma. Anti-MAP4 monoclonal antibody was from Transduction Laboratories (Lexington, KY). Mouse monoclonal anti-kinesin antibody was purchased from Chemicon International (Temecula, CA). Rabbit polyclonal anti-EB1 was from Santa Cruz Biotechnology, Inc. (Santa Cruz, CA), and mouse monoclonal anti-HSP90β antibody was purchased from StressGen Biotechnologies (Victoria, British Columbia, Canada). Both fluorescently labeled and horseradish peroxidase-conjugated secondary antibodies were purchased from Jackson ImmunoResearch Laboratories (West Grove, PA). BSA, DMSO, EGTA, EDTA, PIPES, $MgSO_4$, and sucrose were from BioShop Canada. IFN-γ from *Mus musculus* was from PeproTech. Phosphocellulose-purified bovine brain tubulin (99% pure) was purchased from Cytoskeleton Inc. (Denver, CO). AMP-PNP, paclitaxel, GTP, LPS, mammalian protease inhibitor, hexokinase, geldanamycin, and all other reagents were purchased from Sigma-Aldrich.

Cell Culture, Activation, and Pharmacological Treatment—The RAW264.7 macrophage cell line was obtained from the American Type Culture Collection (Manassas, VA) and maintained at 37 °C supplied with 5% CO_2 in DMEM supplemented with 10% heat-inactivated FBS. Primary macrophages were isolated from the peritoneal cavities of 3-month-old C57BL/6 mice. Briefly resident peritoneal macrophages were harvested from sacrificed mice by peritoneal lavage by injecting 5 ml of ice-cold PBS (without Ca^{2+}/Mg^{2+}) containing 5% heat-inactivated FBS. To prevent activation by glass adherence, macrophages from each mouse were plated separately on poly(L-lysine)-coated coverslips (0.2 mg/ml; overnight, before blocking with 0.1% BSA) and grown in DMEM supplemented with 10% FBS and antibiotics (100 IU/ml penicillin and 100 μg/ml streptomycin) at 37 °C in 5% CO_2 for 2 h before washing away non-adherent cells. Resident peritoneal macrophages or resting RAW264.7 cells were activated by a combination of 100 units/ml IFN-γ and 1 μg/ml LPS for 12 h. Inhibition of HSP90 was performed by incubating resting RAW264.7 cells with 0.1 and 1 μM geldanamycin (GA) for 1 h followed by IFN-γ/LPS (100 units/ml and 1 μg/ml, respectively, for 12 h) stimulation in the presence of the drug.

MT Assembly and Extraction of MAPs—For MAP purification, RAW264.7 macrophages were grown to 80–90% confluence in at least 10 150 $\times$ 20-mm culture dishes ($\sim 5 \times 10^7$ cells/dish). Cells were activated by a combination of 100 units/ml IFN-γ and 1 μg/ml LPS for 12 h in 50% of culture dishes, whereas the remaining 50% were used as corresponding controls. After incubation, both control and activated cells were washed with PBS, harvested, and collected by pelleting. The cells were resuspended in 2 ml of PEM buffer (35 mM PIPES (pH 7.4), 5 mM $MgSO_4$, 0.5 mM EDTA, 5 mM EGTA) containing mammalian protease inhibitor and 1 mM DTT. The cells were subjected to eight passes through a stainless steel ball bearing type homogenizer with a clearance of 12 μm (Isobiotec, Heidelberg, Germany). The homogenates from both control and activated cells were centrifuged at 1,000 $\times$ *g* for 10 min to remove large cell debris, and the resulting supernatants were centrifuged at 12,000 $\times$ *g* for 15 min. The supernatants were again centrifuged at 190,000 $\times$ *g* for 30 min to remove all remaining membranes. The supernatants from control and stimulated cells were collected, and 1 mM GTP, 20 μM Taxol, 7 mM AMP-PNP, 20 units/ml hexokinase, and 10 mM glucose were added. Taxol-stabilized MTs prepared from phosphocellulose-purified bovine brain tubulin were added to a final concentration of 0.7 mg/ml, and the mixture was incubated for 20 min at 37 °C to polymerize endogenous MTs. After incubation for 20 min at 37 °C, the MTs were washed by centrifugation through discontinuous sucrose gradients (100 μl each of 12.5 and 25% sucrose in PEM buffer containing 20 μM Taxol and 1 mM GTP) for 45 min at 115,000 $\times$ *g* at 20 °C. The sucrose cushion removes any contaminating soluble cytoplasmic proteins entrapped in the MTs.

MT pellets were washed in PEM buffer containing 1 mM GTP and 20 μM Taxol, and the MTs were centrifuged at 30,000 $\times$ *g* for 25 min. To dissociate MAPs from MTs, the MT pellets were resuspended in homogenization buffer containing 1 mM GTP and 20 μM Taxol at

37 °C, and NaCl was added to 0.35 M concentration. The solution was centrifuged again at 30,000 × *g* for 25 min, leaving the MAPs in the supernatant. The procedure was adapted from that described for the isolation of brain MT-associated proteins (36). A repeat wash was performed. MT-associated proteins extracted in the supernatant were quantified by DC protein assay kit (Bio-Rad). Typically a total of 150 μg of MAPs were isolated from activated and resting RAW264.7 cells. To assess any potential protein impurities from bovine brain tubulin, MAPs, if any, were also released from 0.7 mg/ml bovine tubulin alone as described above.

Fractionation, Digestion, and LC-MS/MS Analysis of MAPs—55 μg of MAPs obtained from control and IFN-γ/LPS-treated cells were incubated with iodoacetamide to alkylate cysteine residues. DTT in 20 mM HEPES (pH 8) was added (final concentration, 6 mM) to MAPs and incubated at 37 °C for 30 min. Then iodoacetamide was added (final concentration, 10 mM) to react for 30 min at room temperature. MAPs were stored at −20 °C until fractionation. To reduce sample complexity, MAPs were fractionated by reverse-phase chromatography medium (Phenomenex, Jupiter C_4, 300 Å, 2 × 150 mm) using a Waters 2695 Alliance LC system with column temperature at 35 °C, flow rate at 0.45 ml/min, and solvent A (0.1% (v/v) trifluoroacetic acid in water) and solvent B (95% (v/v) acetonitrile and 0.1% (v/v) trifluoroacetic acid). 45 μg of intact MAPs proteins were fractionated by a gradient of solvent B (5, 5, 23, 30, 40, 65, and 95%) at 0, 1, 5, 8.5, 45, 55, 65 min after injection, respectively. Typically 24 fractions (1 ml each) were collected at 135-s time intervals starting after 13 min of injection, and the volumes of fractions were reduced by SpeedVac and then completely dried with a freeze dryer. 35 μl of 1 M ammonium bicarbonate containing 40 ng of modified trypsin (Promega, Madison, WI) were added to adjust pH to ~8.5, resuspend, and digest the proteins overnight at 37 °C. Fifty percent of the digests was loaded onto an HPLC-Chip (160-nl high capacity sample enrichment column and 75-μm × 150-mm SB-C_{18} separation column, Agilent Technologies, Santa Clara, CA) and separated by flow rate at 300 nl/min with solvent A (0.2% (v/v) formic acid in water) and solvent B (90% (v/v) acetonitrile and 0.1% (v/v) formic acid) and the following gradients of 3, 35, 80, and 100% solvent B at 0, 50, 54, and 56 min after injection, respectively. The LC-MS/MS analysis was carried out by an Agilent 1100 HPLC-Chip and 6340 ion trap system with MS scan range from 300 to 1,300 *m/z*. 30-s dynamic exclusion was applied to the precursor previously selected for MS/MS twice. MAPs released from bovine brain tubulin were lyophilized and resuspended in 80 μl of 0.25 M ammonium bicarbonate containing 50 ng of trypsin, digested overnight, and cleaned up by C_{18} StageTip (Proxeon, Odense, Denmark). The digest was analyzed by LC-MS/MS as described above.

Protein Database Search—Raw data files from LC-MS/MS analysis of the 24 fractions were combined to search against Swiss-Prot (Release 56.4) restricted to the mouse subset database (15,941 protein entries) using Spectrum Mill MS Proteomics Workbench (v03.03.082, Agilent Technologies). The Data Extractor utility program detected peaks, assigned precursor charges where possible (for those not successfully determined, 2+ to 5+ were considered), filtered MS/MS spectra by quality (spectra with peak number >4 and sequence tag length >2 were kept for MS/MS search), centroided the MS/MS spectra, merged nearby MS/MS spectra from the same precursor by default MS/MS similarity criteria, and generated peak lists. Peak lists were searched by the following criteria: two missed trypsin cleavages, fixed modification (carbamidomethylation on cysteine), precursor mass tolerance of ±2.5 Da, and product mass tolerance of ±0.7 Da. After the search, the spectra and protein identities were validated (see below) and tagged as "valid," and a second search was performed for spectra with no valid tag to identify spectra with oxidized methionine and pyroglutamic acid modification at N-terminal glutamines. The mouse database used for the second search was further restricted to those proteins tagged as valid from the first search. The search result was validated the same as described below.

Criteria to Report Protein and Peptide Identification and Estimation of False Positive Rate—Using SpectrumMill Autovalidation tool and its default settings (see below), spectra and protein identities fulfilling the following scoring threshold criteria (both the "Protein detail" and "Peptide" modes) were determined and labeled as valid. Parameters for the Protein detail mode were: protein score, >20; peptide score, scored percent intensity, delta rank1 − rank2, delta forward − reverse, respectively: peptide charge +2, >6, >60%, >2, >2; peptide charge +3, >8, >70%, >2, >2; peptide charge +4, >8, >70%, >2, >2; peptide charge +5, >12, >70%, >2, >2; peptide charge +2, >6, >90%, >1, >1. Parameters for the Peptide mode were: peptide score, scored percent intensity, delta rank1 − rank2, delta forward − reverse, respectively: peptide charge +2, >11, >60%, >2, >2; peptide charge +3, >13, >70%, >2, >2; peptide charge +4, >13, >70%, >2, >2; peptide charge +5, >15, >70%, >2, >2. The software groups the proteins together when a peptide sequence longer than eight residues is contained in multiple protein entries in the sequence database and reports the highest scoring one and its accession number. Based on the above grouping rule and these threshold criteria, 327, 378, and 397 protein groups were considered as valid in three biological replicates of activated samples, and 377, 401, and 402 protein groups were considered as valid in three control samples. The false positive rate for the above validating criteria was estimated by repeating the same process except using the database with all of the protein sequences reversed. The number of proteins that passed these thresholds was used to calculate the false positive rate. 7–14 proteins were identified by the reverse database method; thus the estimated overall false positive identification rates are 2.1–3.5% among six LC-MS/MS runs.

Data Analysis—Proteins identified after database searches were subjected to additional filtering criteria to further minimize false positive identifications. Proteins identified in only one of the three independent LC-MS/MS measurements were excluded. In addition, only proteins with at least two unique peptides in three independent LC-MS/MS measurements were classified as positively identified. A unique peptide was defined as the following: a particular peptide identified by multiple MS/MS spectra due to different precursor charge states, distribution among adjacent fractions, and modifications that occurred during protein handling (oxidized methionine and pyroglutamic acid at N-terminal glutamine were considered in this study). The highest scored MS/MS spectrum was used to report the score of the unique peptide and to calculate the total MS/MS score for the proteins reported in supplemental Table 1.

The relative protein abundance was estimated based on the number of all MS/MS spectra representing identified peptides for a given protein. To quantify changes in spectral counts, we estimated -fold changes after normalization of spectral count using the following formula, which avoids the discontinuity seen in the simple count ratios when a protein shows a spectral count of 0 in one of the samples. The spectral counts for each protein were normalized according to total spectral counts for all the proteins in the samples (37, 38). In this instance, t_1 was the total spectral counts for all the proteins in the control sample, t_2 was the total spectral counts for all the proteins in the activated sample, n_1 was the spectral count for the protein in the control sample, and n_2 was the spectral count for the protein in the activated sample. Thus, for each protein

$$f_1 = n_1\frac{t_2}{t_1} + \lambda \qquad \text{(Eq. 1)}$$

and

$$f_2 = n_2 + \lambda \qquad \text{(Eq. 2)}$$

where λ is the pseudo spectral count (=0.5 in this case). The pseudo spectral count is used here to avoid taking the logarithm of zero values. The spectral count for a given protein was the average of individual spectral counts from three replicate LC-MS/MS measurements after normalization. Protein relative abundances refer to the ratio of the spectral count of MAPs obtained from IFN-γ/LPS-treated cells (f_{-2}) relative to that of the spectral count from control reference (f_{-1}). To determine whether a protein was more abundant in MAPs obtained from activated macrophage samples than MAPs obtained from the control resting macrophage samples, we used the two-tailed Student's *t* test to test whether the mean base 2 logarithmic ($\log_2$) values of the ratios of spectral count (f_{-2}/f_{-1}) of the same protein are different from zero. Protein abundance was only considered significant if the *p* value was <0.05. Proteins that passed the *t* test with positive mean $\log_2$ values were considered more abundant in one sample, whereas proteins that passed the *t* test with negative mean $\log_2$ values were considered more abundant in the other sample. Proteins that did not pass the *t* test were considered insignificant with regard to their relative abundance in samples. Data were expressed as mean ± S.E. All calculations were performed using a desktop spreadsheet program (Excel, Microsoft, Redmond, WA).

Transmission Electron Microscopy (TEM)—Pellets containing Taxol-stabilized MTs from IFN-γ/LPS-treated cells were resuspended in PEM buffer. Protein samples at 1.0 mg/ml were adsorbed for 10 s on carbon- and Formvar-coated copper grids (Electron Microscopy Sciences, Hatfield, PA) and negatively stained with 1% uranyl acetate in double distilled water. Electron microscopy was performed using a transmission electron microscope (Philips Electronic Instruments, Inc., Mahwah, NJ).

Immunofluorescence and Epifluorescence Microscopy—For visualization of the endogenously expressed MT-associated proteins, resident peritoneal macrophages and RAW264.7 macrophages were grown on coverslips in 6-well plates overnight. Control as well as stimulated cells (100 units/ml IFN-γ and 1 μg/ml LPS for 12 h) were washed with PBS, fixed, and immunostained as described previously (39). The primary antibody (Ab) dilutions used were: acetylated tubulin, 1:1,000; α-tubulin, 1:10,000; MAP1, 1:500; MAP4, 1:1,000; talin, 1:2,000; kinesin, 1:1,000; dynein, 1:1,000; EB1, 1:500; and HSP90β, 1:2,000. Incubation with primary Abs was followed by incubation with the corresponding fluorochrome-conjugated secondary Ab. After mounting, samples were analyzed by an Axiovert 200M microscope equipped with differential interference contrast and epifluorescence optics (Carl Zeiss Microimaging Inc.). RAW264.7 cells treated with geldanamycin were also fixed and processed for immunostaining as described above.

Protein Electrophoresis and Western Blot Analysis—Total protein as well as the isolated MAPs obtained from resting, IFN-γ/LPS-treated cells and bovine brain tubulin were dissolved in Laemmli buffer and boiled for 5 min. Equal protein amounts were loaded and analyzed by SDS-PAGE and Western blotting as described previously (40). Protein detection was performed by exposing nitrocellulose membrane to the primary antibodies acetylated tubulin (1:5,000), MAP1 (1:500), MAP4 (1:1,000), talin (1:2,000), α-tubulin (1:10,000), kinesin (1:1,000), dynein (1:1,000), EB1 (1:500), β-actin (1:1,000), and HSP90β (1:3,000). Immunodetection was performed using corresponding secondary antibodies conjugated to horseradish peroxidase (diluted 1:1,000). Blotting was visualized by the ECL Western blotting detection system (Amersham Biosciences) according to the manufacturer's instructions. Total lysates from macrophage cells without and with geldanamycin treatment in the presence of IFN-γ/LPS were also immunoblotted as described above. Protein bands were measured by densitometry scanning of independent experiments using NIH/Scion Image software, and relative pixel intensities were normalized between experiments. Pooled values between experiments were expressed as mean ± S.E. -fold activation/induction or reduction of association of proteins compared with control experiments.

Bioinformatics Analysis—MS identities were received in the form of Swiss-Prot database accession numbers. Proteins encoded by genes were classified according to their function in the Gene Ontology database (41) supported by manual data mining of references in the Swiss-Prot database. Unknown proteins were those that have not been investigated previously. Known interactions between mouse proteins were downloaded from InteroPorc, which stores known interactions combined from the Database of Interacting Proteins, Molecular Interactions Database, and IntAct interaction database. Redundancy and self-interactions were removed, giving a data set of 5,708 pairwise interactions. This file was parsed using in-house Perl scripts to identify direct interactions between MAPs. Because fewer direct interactions were identified between mouse MAPs than expected and it is assumed that protein-protein interactions are largely conserved between human and mouse, human interaction data were utilized to identify further interactions between MAPs. BLASTp searches were carried out to find homologues in the human proteome and downloaded from Integr8 using a reciprocal best hits technique. Each mouse MAP was aligned against the human proteome and the lowest e-value, or "best," scoring hit was stored with a cutoff e-value of 10^{-10}. These "best bits" were then aligned against the mouse proteome, and if the best hit was reciprocal the proteins were considered to be homologous. On occasion, one mouse protein would match to more than one homologous human protein, each with the same best score; in these cases, all homologous proteins were stored. Interactions were then identified between these human proteins, further utilizing known interaction data from InteroPorc, and mapped back to the previously established mouse homologues. All networks were visualized using the Osprey Network Visualization Tool (v1.2.1) (42) where nodes represent proteins and edges represent interactions. To determine whether the MAP set contained significantly more direct pairwise interactions than a group of randomly selected proteins, an in-house Perl script was used to construct random sets of either human or mouse proteins separately and count the pairwise interactions within that set. A total of 1,000 repeats were run to achieve and plot a distribution of the data. The one-sample *t* test was used to determine whether the MAP set had significantly more interactions than the random set.

RESULTS

Activated Macrophages Display Rapidly Stabilized MT Subsets—We reported previously that activation of macrophages with the inflammatory mediator IFN-γ promotes stabilization of MTs (39). Furthermore we showed that classical activation of macrophages with IFN-γ and LPS enhances cell spreading and particle binding necessary for enhanced killing during inflammatory events. We examined MT stabilization in the macrophage cell line RAW264.7 activated with IFN-γ and LPS (100 units/ml and 1 μg/ml, respectively). This cell line undergoes robust phagocytosis and activation and can be grown to high yields for detailed molecular and biochemical analysis of macrophage functions. MT stabilization was monitored using an anti-acetylated α-tubulin antibody (43, 10). Activated macrophages were larger and more spread as reported previously (5). Indirect immunofluorescence (IF) analysis with the anti-acetylated α-tubulin antibody (Fig. 1*A*) revealed an increase in acetylated MTs in IFN-γ/LPS-treated cells compared with control cells, which had very low levels of acetylated tubulin

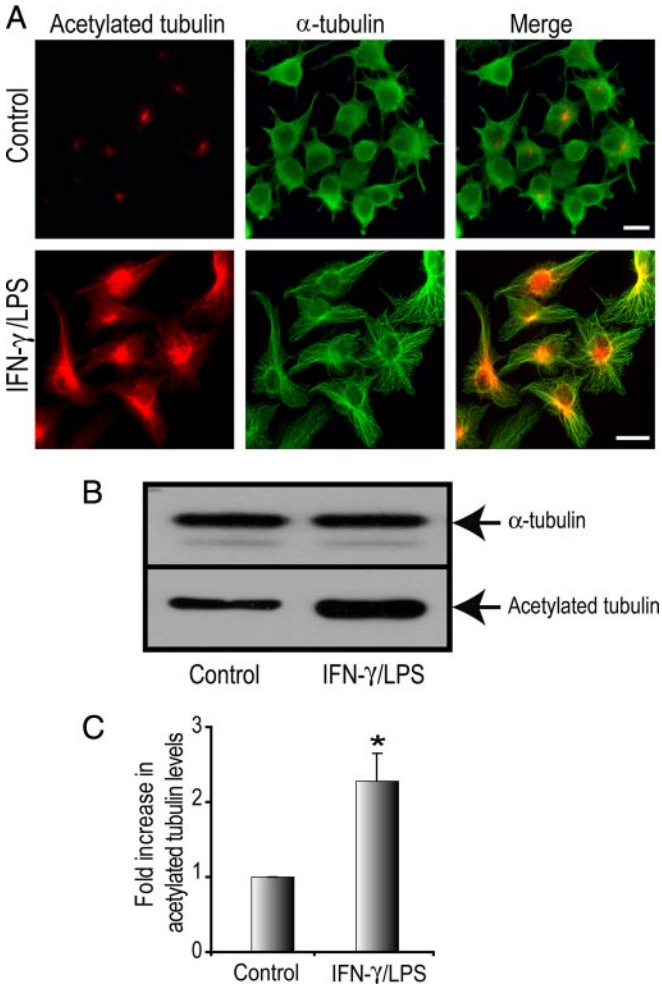

FIG. 1. **Macrophages activated with IFN-γ plus LPS exhibit increased levels of stable MTs.** RAW264.7 cells were stimulated with IFN-γ/LPS (100 units/ml and 1 μg/ml, respectively, for 12 h) or left untreated. *A*, cells were fixed and immunostained for acetylated tubulin (*red*) and α-tubulin (*green*). *Scale bar*, 10 μm. *B*, Western blot analysis of total cell lysates. A representative Western blot shows the acetylated tubulin and total α-tubulin levels in resting and IFN-γ/LPS-treated RAW264.7 cells. *C*, densitometric analysis revealed a substantial and significant increase in acetylated tubulin levels in IFN-γ/LPS-treated macrophages compared with control macrophages. Data is expressed as mean ± S. E. ($n = 3$). * indicates $p < 0.05$.

(Fig. 1*A*). Cells were co-stained with a polyclonal α-tubulin antibody to demarcate the total MT population in these cells. Western blotting analysis for acetylated tubulin and total α-tubulin levels in control and IFN-γ/LPS-treated macrophages revealed an increase in stabilized MTs after activation (Fig. 1*B*). Following quantification, we observed a statistically significant increase in acetylated tubulin levels, 2.4-fold higher in IFN-γ/LPS-treated RAW264.7 cells, compared with control cells (Fig. 1*C*). These results confirmed that macrophage activation resulted in a dramatic and rapid modulation of the MT cytoskeleton (5, 39). We next sought to identify the entire MT protein complement in macrophages before and after classical activation.

Shotgun Proteomics Analysis of MAPs from RAW264.7 Macrophages and Quantitative Analysis by Spectral Counting—We identified macrophage MAPs using a mass spectrometry-based method. MAPs were purified from murine RAW264.7 macrophage cells using a previously described MT co-sedimentation assay (36, 44, 45). This procedure involves the stabilization of MTs by Taxol and is schematically depicted in Fig. 2. MT fractions obtained using Taxol are known to contain MAPs that promote tubulin assembly (36, 44, 45). Cell lysates of untreated and IFN-γ/LPS-treated RAW264.7 macrophages were incubated in the presence of GTP to promote the polymerization of endogenous MTs along with Taxol-stabilized exogenous bovine tubulin in the presence of AMP-PNP, glucose, and hexokinase to strengthen binding of motors to MTs (46, 47). The assembled MT network, prior to MAP depletion, was examined by TEM analysis. Fig. 3*A* displays the longitudinal structure of macrophage MTs. Higher magnification images reveal electron-dense structures, which are likely associated ribosomes (19). Because MAPs have been shown to dissociate from Taxol-stabilized MTs at high ionic strengths (36), MAPs were released from Taxol-stabilized MTs upon incubation in homogenization buffer containing 0.35 M NaCl (Fig. 2). MAPs were also released similarly from pure bovine brain tubulin to determine whether there was any contamination of exogenous MAPs in the sample preparations. A sample one-dimensional SDS-PAGE gel displays MAPs isolated from control, activated macrophages, and bovine brain tubulin (Fig. 3*B*). The amounts of silver-stainable proteins in both control and IFN-γ/LPS-treated lanes were similar and obviously higher than that in the bovine tubulin lane, indicating successful MAP isolation and very few contaminating proteins in the bovine tubulin preparation. The MAPs obtained from control and IFN-γ/LPS-treated macrophage were fractionated by C_4 reverse-phase LC (48). In total, 24 fractions were digested with trypsin and analyzed by C_{18} reverse-phase LC-MS/MS. Proteins were identified by searching a mouse subset of the Swiss-Prot database (Release 56.4). In this study, we isolated MAPs from control and IFN-γ/LPS-treated macrophages in triplicate, thus resulting in a total of three biological replicates. Compilation of the data from all three analyses resulted in the identification of 409 MT-associated proteins from macrophages (supplemental Table 1). These MAPs were proteins that were observed in at least two of the three analyses with at least two unique peptides. As a result of this further restriction, the false positive rate of the analyzed MAPs was smaller than the estimated 2.1–3.5% based on the reverse database search. MAP analyses of bovine brain tubulin revealed only two proteins, which were tubulin isoforms, validating the purity of the exogenous tubulin added (supplemental Table 1, indicated by asterisks).

To classify the 409 proteins on a functional basis, we first characterized the comprehensive data set of MAPs according to the Gene Ontology database (41) supported by additional manual data mining of previously published work (Fig. 3*C* and

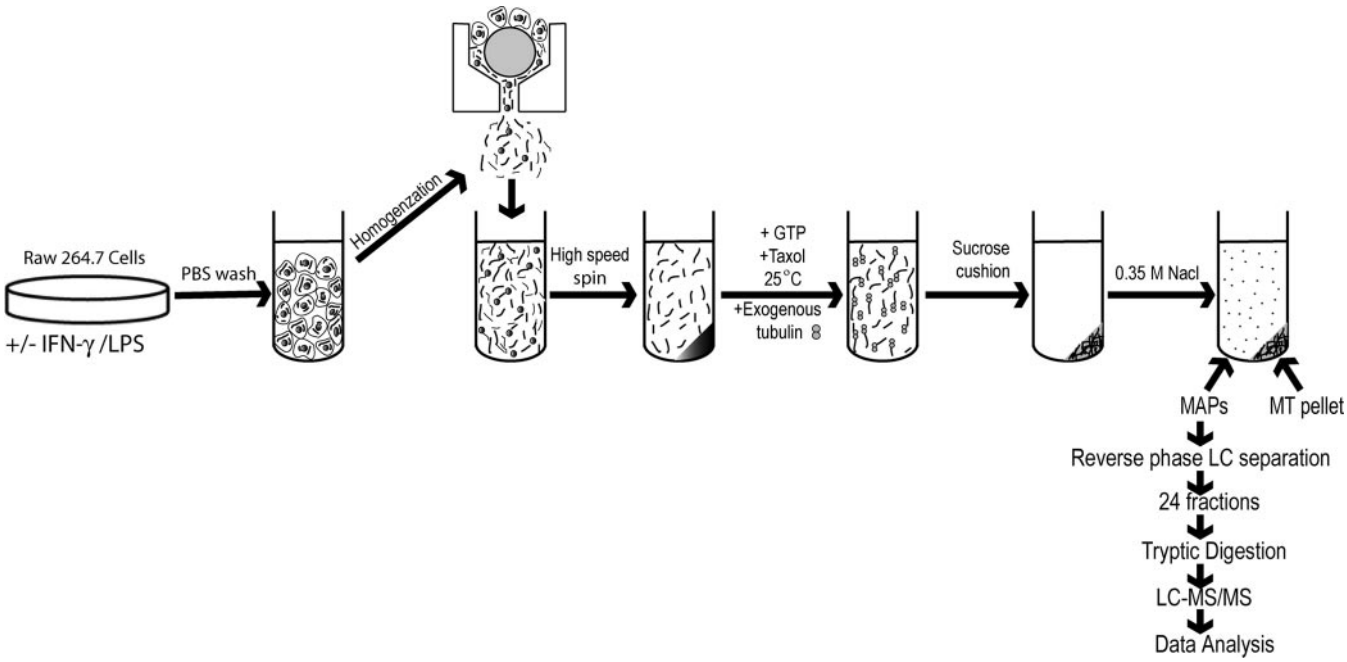

FIG. 2. **Schematic representation of the protocol used for purification of MAPs from RAW264.7 cells.** Control and activated macrophages were mechanically lysed, and following a high spin, MTs and MAPs were co-sedimented in the presence of Taxol, GTP, AMP-PNP, and exogenous tubulin. MAPs were dissociated from Taxol-stabilized MTs at high ionic strengths. The MAPs obtained from both resting and IFN-γ/LPS-treated macrophage cells were fractionated by reverse-phase liquid chromatography. Fractions from each sample were digested with trypsin and analyzed by C_{18} reverse-phase LC/MS/MS. Proteins were identified by searching a mouse subset of the Swiss-Prot database as described under "Experimental Procedures."

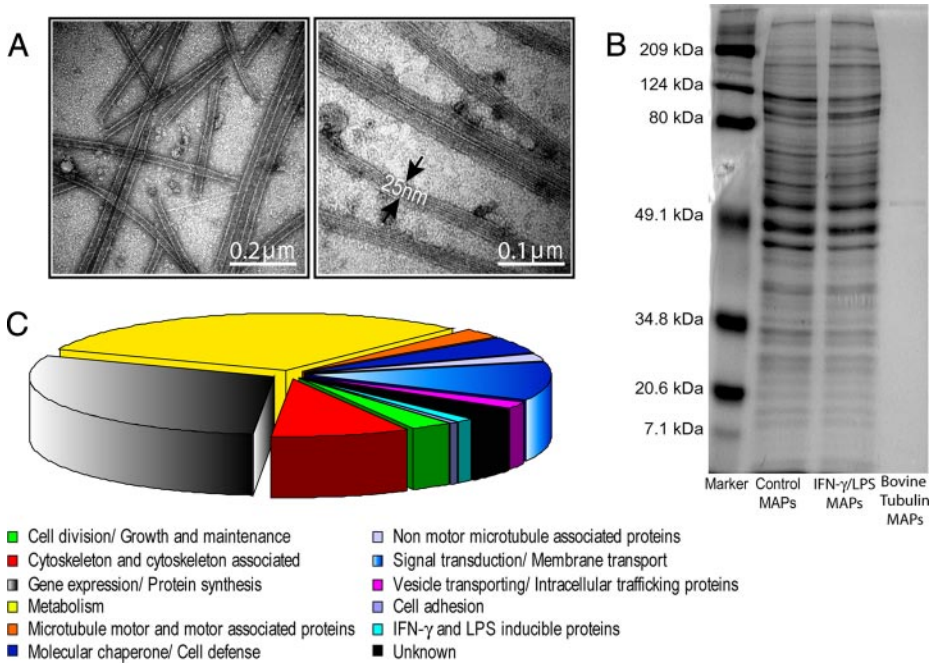

FIG. 3. **Morphological and molecular characterization of MTs and MAPs from macrophages.** *A*, negatively stained electron micrographs of MTs from IFN-γ/LPS-treated RAW264.7 cells. *Arrows* outline the walls of the MTs. *B*, one-dimensional gel electrophoresis of purified MAPs isolated from resting and IFN-γ/LPS-treated RAW264.7 cells and from commercial bovine brain tubulin alone. *C*, functional classification of 409 MAPs from IFN-γ/LPS-treated RAW264.7 cells. A pie chart shows the classification of identified MAPs according to the Gene Ontology database assisted by additional manual data mining of previously published work. MAPs were categorized into 12 different categories based on their cellular functions.

supplemental Table 1). In macrophages containing a total of 409 MAPs, 2.93% (12 proteins) of proteins were annotated as cell division/growth and maintenance, 0.49% (two proteins) were annotated as cell adhesion, 8.56% (35 proteins) were annotated as cytoskeleton and cytoskeleton-associated protein, 2.69% (11 proteins) were annotated as MT motors and motor-associated proteins, 2.20% (nine proteins) were annotated as non-motor MT-associated proteins, 31.30% (128) were proteins involved in various metabolic pathways, 29.83% (122) were proteins involved in gene synthesis/pro-

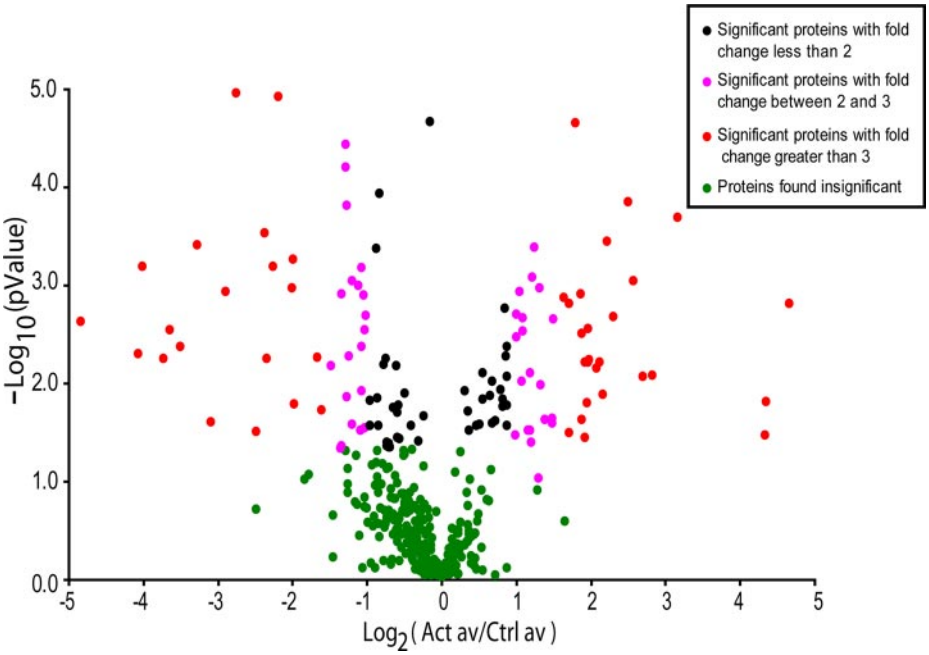

FIG. 4. **Graphical representation of quantitative proteomics data of MAPs purified from resting and IFN-γ/LPS-treated macrophages.** A volcano plot was generated by plotting the *t* test *p* value against the relative abundance ratio between IFN-γ/LPS-treated and control samples on a logarithmic scale. From a total of 409 identified proteins, 140 proteins were significant in differential expression ($p < 0.05$). Among them, 46 proteins had less than a 2-fold change (*black dots*), 41 proteins had a -fold change between 2 and 3 (*pink dots*), and 53 had greater than a 3-fold change (*red dots*). Of these, 52 were up-regulated 2-fold or greater, and 42 were down-regulated 2-fold or greater after IFN-γ/LPS stimulation. The remaining 269 proteins did not show a significant difference in expression levels ($p > 0.05$; *green dots*). *Act av*, activated average; *Ctrl av*, control average.

tein expression, 11.98% (49 proteins) were annotated as signal transduction/membrane transport proteins, 4.65% (19 proteins) were annotated as molecular chaperone/cell defense, 0.98% (four proteins) were proteins involved in vesicle transport, 1.22% (five proteins) were proteins that are known to be induced by IFN-γ and LPS treatment, and 3.18% (13 proteins) were proteins with unknown functions (Fig. 3*C*).

In addition, the effect of macrophage activation on MT-associated proteins was determined by examining the number of proteins that are differentially expressed between control and IFN-γ/LPS-treated samples using a -fold test. For this analysis, -fold change refers to the ratio of relative abundance of a protein in the IFN-γ- and LPS-treated *versus* control samples (f_2/f_1). A two-sample *t* test (assuming equal variances) was performed to determine whether the observed differential expression of these proteins was significant or not. We used a volcano plot in Fig. 4 to visualize the differentially expressed proteins based on the simple 2- and 3-fold change threshold and displayed their statistical significance based on their *t* test with peptide level abundance. In the volcano plot, the *t* test *p* value was plotted against the relative abundance ratio between IFN-γ/LPS-treated and control samples on a logarithmic scale. Of the 409 proteins, 140 proteins showed significant differential expression as indicated by the *t* test (Fig. 4, $p < 0.05$). Among them, 46 proteins had less than a 2-fold change (*black dots*), 41 proteins had a -fold change between 2 and 3 (*pink dots*), and 53 had greater than a 3-fold change (*red dots*). The remaining 269 proteins did not show a significant difference in expression levels ($p > 0.05$; *green dots*). Our study thus demonstrates that macrophage activation by IFN-γ/LPS modulates many MAPs mainly through enhanced MT binding. However, a significant number of MAPs are released from MTs during this process. This suggests a complex pattern of MAP regulation during IFN-γ/LPS macrophage activation.

Bioinformatics Analysis of Binary MAP Interactions—The proteins identified in this study were isolated because of their association with MTs. This common property of the proteins led us to predict that they interact with one another at a higher frequency than a set of randomly selected, unrelated proteins. To test this hypothesis, we utilized protein-protein interaction data stored in the InteroPorc database, which stores known physical interactions combined from the Database of Interacting Proteins, Molecular Interactions Database, and IntAct interaction database. These interactions were parsed using in-house Perl scripts to remove self-interactions and to store proteins by their Swiss-Prot accession codes. An interaction data set of 5,708 pairwise interactions was collected for mouse. Of our 409 MAPs identified from macrophages, in-house computer algorithms identified available interaction data for 218. An analysis of the binary protein interactions between these proteins identified 206 interactions within the

set of MAPs when considering "A-B" and "B-A" each as one interaction. Because fewer direct interactions were identified between MAPs than expected, the vast amount of human interaction data was utilized. It was assumed that protein-protein interactions are largely conserved between mouse and human; thus by identifying homologues between the two species, additional interactions could be mapped across to mouse. By using a BLAST-based reciprocal best hits approach with an e-value cutoff of 10^{-10}, 659 human homologues were identified from the 409 mouse MAPs. Of these human proteins, 422 possessed any interaction data from a human interactome collated from InteroPorc, resulting in 784 pairwise interactions between MAPs. Interactions were mapped back to mouse using the previously established homologues, and an overall interaction network was constructed using both the mouse and human interactions containing 234 proteins with 461 interactions between them (Fig. 5*A*).

To determine whether the MAP set contained significantly more direct pairwise interactions than a group of randomly selected proteins, an in-house Perl script was used to construct a random set of *mouse* proteins and to count the pairwise interactions within that set (17). A total of 1,000 repeats were carried out to achieve and plot a distribution of the data (Fig. 5*B*). As 218 of the 409 MAPs show any interactions at all in the InteroPorc data, sets of size 218 were used when searching the mouse proteins, resulting in an average of 31 interactions (S.D., ±18.28; $n = 1{,}000$). This indicates that the set of MAPs interact with one another at significantly higher frequency than a random set of proteins ($p < 0.0001$). A similar test was carried out using human interaction data using sets of size 422, resulting in an average of 103 interactions (S.D., ±29.87; $n = 1{,}000$; Fig. 5*B*). The number of interactions between MAPs is significant in comparison with a random set ($p < 0.0001$).

Confirmation of Proteomics Results by Western Blot and IF Analysis—To corroborate the results obtained by the LC-MS/MS approach, we quantified the levels of seven differentially expressed proteins, kinesin, dynein, MAP1, MAP4, EB1, HSP90β, and talin, in control and IFN-γ/LPS-treated macrophages. α-Tubulin was used as a control for sample loading. Antibodies against talin (~230 kDa), kinesin (~120 kDa), dynein (~70 kDa), MAP1 (~325 kDa), MAP4 (~220 kDa), EB1 (~34 kDa), and HSP90β (~90 kDa) were used to visualize bands of expected molecular masses in both control and IFN-γ/LPS-treated samples (Fig. 6*A*). The signals obtained with these antibodies were stronger in IFN-γ/LPS-treated samples compared with control samples. Measurement of band density using ImageJ software (National Institutes of Health, Bethesda, MD) indicated a 2–3.5-fold increase in expression levels of these proteins in IFN-γ/LPS-activated macrophages (Fig. 6*B*). Thus, Western blot analysis confirmed the identity of these proteins and their increase within the MAP fraction observed by MS analysis, although the -fold changes obtained by the two approaches were not identical. Additionally we analyzed localization of these up-regulated MT proteins in RAW264.7 macrophages and resident peritoneal macrophages without and with IFN-γ/LPS-treatment using IF. Partial co-localization of these proteins was observed in both resting and IFN-γ/LPS-treated macrophages, although overlap was more evident in activated macrophages (RAW264.7 cells and peritoneal macrophages), which were larger and more spread than unstimulated cells (Fig. 7 and see supplemental Fig. 1). Several pieces of evidence suggest that MAP1, MAP4, and EB1 play a significant functional role in stabilizing MTs (49–51); however, the role of HSP90β in stabilizing MTs is not as clear.

Inhibition of HSP90 by GA Reduces MT Stabilization in Activated Macrophages—It has been reported previously that HSP90 can bind tubulin (52, 53). To determine whether HSP90 has a role in MT dynamics in activated macrophages, we used GA to inhibit HSP90 function. As shown in Fig. 8*A*, RAW264.7 cells treated with IFN-γ/LPS induced the formation of stabilized MTs; however, in contrast, HSP90 inactivation by GA disrupted the IFN-γ/LPS-induced stabilization of MTs. Further Western blot analysis demonstrated that treatment of macrophages with GA reduces total acetylated MTs in IFN-γ/LPS-stimulated macrophages in a dose-dependent fashion (Fig. 8*B*). These results indicate that HSP90 plays a critical role in the regulation of MT dynamics in activated macrophages.

DISCUSSION

In this study, we revealed the composition of MAPs in a mammalian cell that rapidly modulates its MT cytoskeleton to perform acute and essential immune functions. Activated macrophages increase in size, and phagocytic, secretory, and migratory capacities increase within hours of stimulation (54–64). We have shown previously that rapid interphase MT stabilization is concomitant with macrophage activation (5, 39). We revealed 409 proteins that associate with MTs in macrophages and identified multiple proteins that show preferential recruitment to MTs depending on the activation status of macrophages. The MAPs identified in our MT proteomics profiling were grouped according to their primary functions as cell adhesion, cell division/growth and maintenance, cytoskeleton and cytoskeleton-associated, MT motor and motor-associated, non-motor MT-associated, and signaling proteins and proteins that are involved in vesicle trafficking or IFN-γ/LPS-inducible proteins. Our analysis also resulted in identification of MT proteins with unknown functions.

The wide range of MAPs identified in macrophages is not surprising given the number of cellular processes that are regulated by MTs including vesicle trafficking, organelle positioning, signal transduction as well as adhesion, migration, cell division, and phagocytosis (65–67). Similar to what has been observed in other published MT proteomes, we observed many "housekeeping" RNA elements and proteins

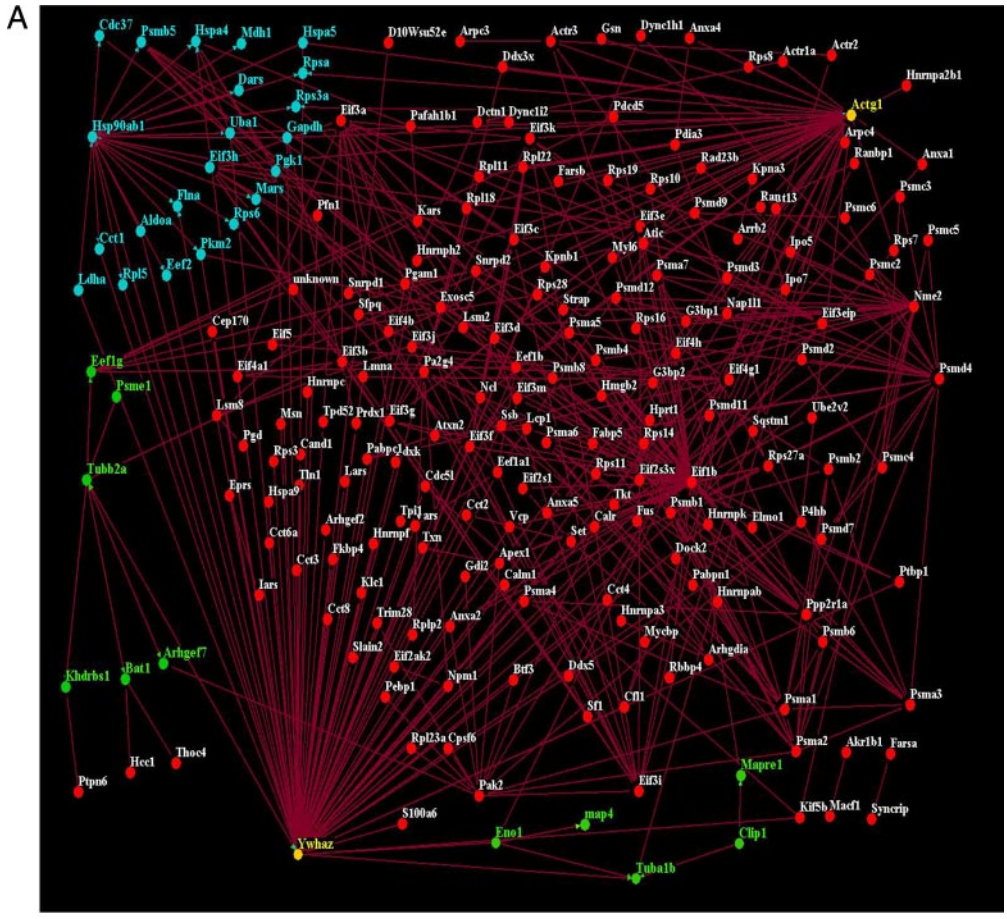

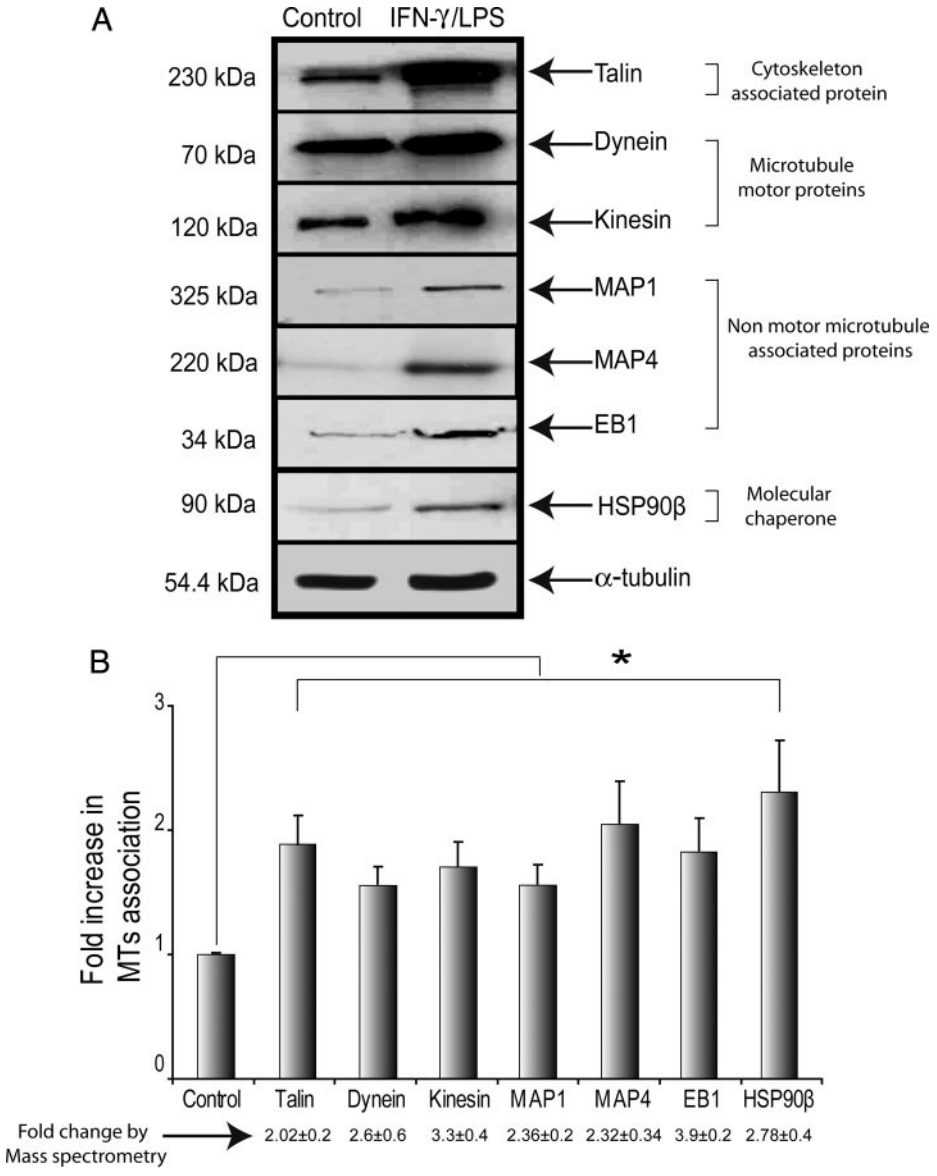

FIG. 6. **Validation of protein expression data by immunoblotting analysis of resting and IFN-γ/LPS-treated macrophages.** *A*, purified MAPs from resting and IFN-γ/LPS-treated RAW264.7 cells were used in Western blot analysis. α-Tubulin was used as an equal loading control. *B*, graph showing the relative expression levels (mean ± S.E.) of MAPs from IFN-γ/LPS-treated and resting macrophage cells. Densitometric analysis revealed a substantial increase in dynein, kinesin, MAP1, MAP4, EB1, talin, and HSP90β protein levels in MAPs isolated from IFN-γ/LPS-treated macrophages compared with control macrophages. Values *below* the graph (mean ± S.E.) represent the -fold change in protein expression based on mass spectrometry analysis. -Fold change values used here are non-logarithmic. * indicates $p < 0.05$.

associating with MTs that are involved in gene expression and metabolism (17, 19–21). Our TEM analysis of purified MTs revealed dense structures that likely represent ribosomes along the MTs. We observed numerous transcription- and translation-related proteins in our macrophage MAP preparations (supplemental Table 1). The precise function of MT-associated ribosomes remains unknown. However, treatment of cells with MT-depolymerizing agents disrupts membrane-bound ribosomes and blocks the reinitiation of protein synthesis, which affects mRNA production and localization (68). This suggests that microtubules partition ribosomes within the cell and potentially translocate them from one place to the other depending on the cell signal. Several researchers have described a role for MTs as a platform for mRNA translation and as a transport conduit for mRNA transcripts to distinct cellular locations (69–71). Similarly clustering of housekeep-

FIG. 5. **Pairwise interactions of MAPs identified from macrophage cells.** *A*, a total of 224 of the 409 MAPs show direct pairwise interaction with another MAP using homologous interactions from human interaction data. Of the 409 MAPs, 206 show direct pairwise interactions when using mouse interaction data. The combination of these binary interactions are displayed here as an interaction network using the Osprey Network Visualization System (v1.2.1). Proteins are indicated by *circular nodes*, and interactions are indicated by *lines*. *Green nodes* represent proteins interacting with tubulin α and β subunits; *blue nodes* represent proteins interacting with HSP90β, and *yellow nodes* indicate interaction with both. *B*, the distribution of interactions within randomly selected sets of proteins gives an average of 103 (S.D., ±29.87; 1,000 repeats) using human interactions and 31 (S.D., ±18.28, 1,000 repeats) using mouse interaction data. The MAP set gave significantly more interactions compared with the random set in both cases.

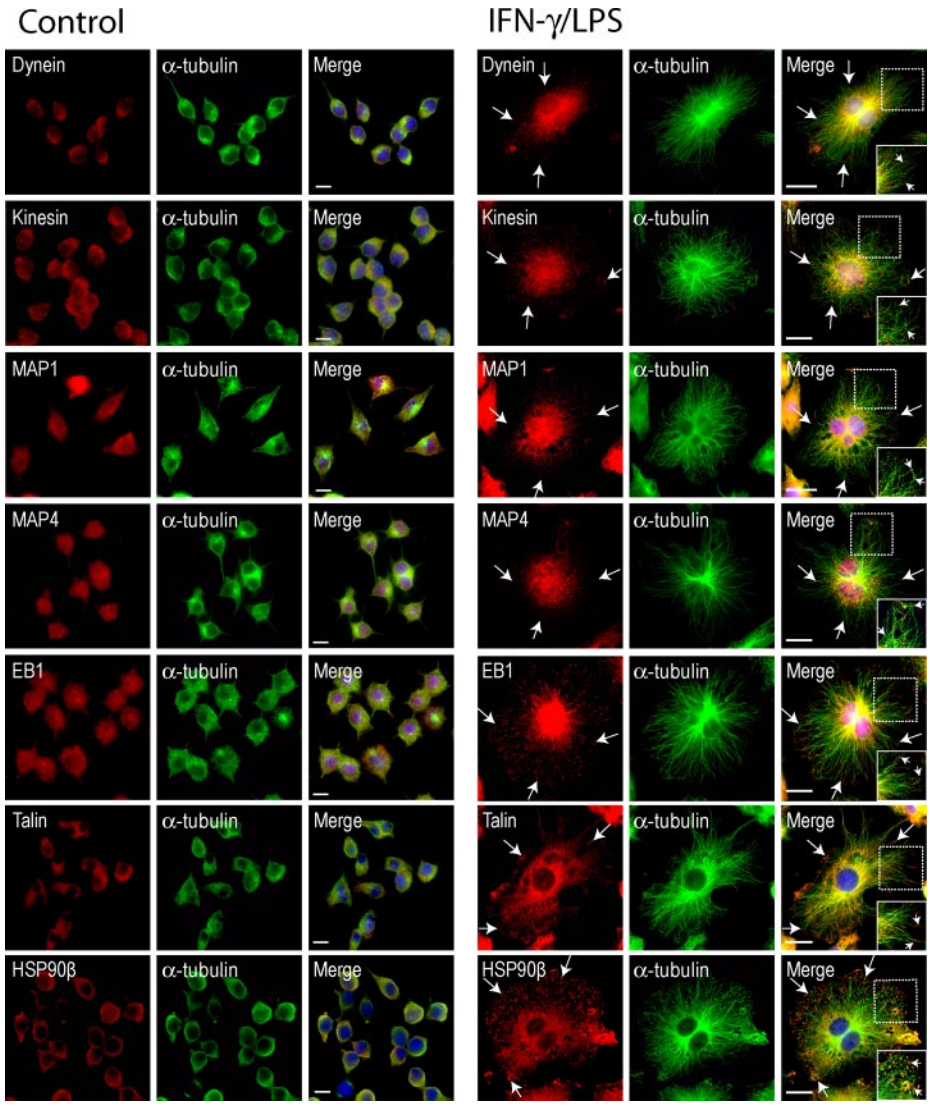

FIG. 7. **Cellular localization of MAPs in RAW264.7 cells.** RAW264.7 cells without and with IFN-γ/LPS stimulation were fixed and immunostained for dynein, kinesin, EB1, MAP1, MAP4, EB1, talin, and HSP90β (indicated in *red*) and total α-tubulin (in *green*). The *boxed region* is shown at a higher magnification in the *inset* (*lower right*). *Arrows* indicate partial co-localization of proteins on MTs. *Scale bars*, 10 μm.

ing enzymes along the MT cytoskeleton provides a means for specific, ordered interactions according to the cellular metabolic needs. Protein degradation machinery has also been reported to be a component of the MAP repertoire (19–21). Of immunological significance, we observed enhanced association of the proteasome elements LMP2/proteasome subunit β type-2 and proteasome activator complex subunit 1/interferon-γ up-regulated I-5111 (IGUP I-5111) protein with MTs in IFN-γ/LPS-activated macrophages (supplemental Table 1) that are critical for major histocompatibility complex (MHC) I antigen processing (72–75). The IGUP I-5111 protein contains an MT binding domain homologous to the MAP1B binding domain (76); however, this is the first report confirming its MT association.

Also similar to other MT proteome studies, we observed numerous F-actin-binding proteins in our MS analysis (18, 20, 21), indicating cytoskeletal cross-talk in macrophages. One protein identified was MT-actin cross-linking factor 1, which contains actin as well as MT binding domains (77) and which may be a key attachment point between MTs and microfilaments. The dynamic nature of phagocytosis and migration in macrophages relies heavily on both F-actin and MTs (39, 78, 79), likely explaining the strong physical and functional interplay between these polymers. For instance, talin is a key regulator of αIIbβ3 integrin activation in activated macrophages necessary for phagocytosis of C3bi-coated target particles (80), and we observed enhanced association of this actin-binding protein with MTs in activated macrophages (Figs. 6 and 7 and supplemental Fig. 1 and Table 1).

Analysis of a single mammalian cell type before and after MT stabilization allowed comparative analysis of the regulation of the MT proteome. In this study, we demonstrated that macrophages produce significant levels of acetylated MTs following classical activation with IFN-γ/LPS. MT acetylation may regulate protein association with MTs in macrophages as tubulin posttranslational modifications have been shown to

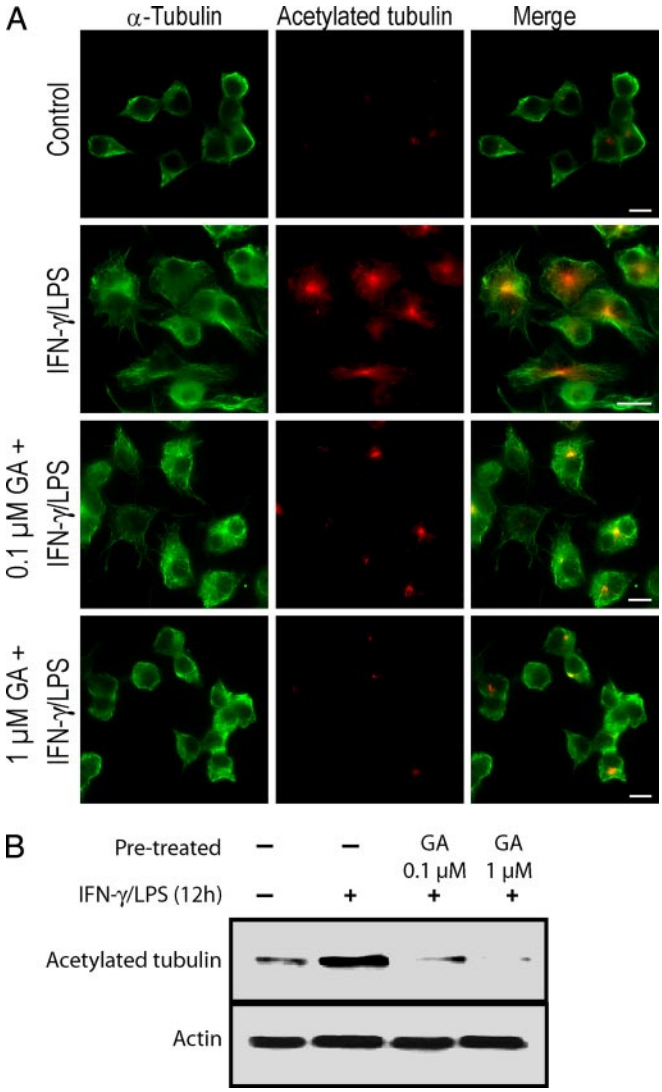

FIG. 8. **HSP90 inactivation reduces stabilization of MTs in IFN-γ/LPS-treated macrophages.** RAW264.7 cells were treated with 0.1 and 1.0 μM GA for 1 h followed by IFN-γ/LPS stimulation or were left untreated. *A*, cells were fixed and immunostained for acetylated tubulin (*red*) and α-tubulin (*green*). *Scale bars*, 10 μm. *B*, Western blot analysis of acetylated tubulin in cell lysates of resting as well as IFN-γ/LPS-treated macrophages with and without GA. Data is expressed as mean ± S. E. ($n = 3$).

enhance binding of motors to MTs (11, 12). We observed enhanced binding of various light and heavy chains of cytoplasmic dynein and kinesin with MTs in activated macrophages. Pronounced vesicle trafficking occurs in activated macrophages to facilitate cytokine, matrix metalloproteinase, and MHC delivery to the cell periphery and to assist in inward movement of phagosomes (32, 81–83). This is the first evidence that there is a quantitative increase in motor association with MTs in activated macrophages that is likely driving these important intracellular movements.

During this study we were able to predict protein-protein interactions between MAPs utilizing both mouse and human interaction data. Because the proteins have all been identified based on their association with MTs, we predicted that they would have significantly more interactions with one another than a randomly selected set of proteins. This was found to be the case using both mouse interactions and human interactions between MAP homologues. This approach was able to further verify the functional relevance that the MAPs identified here have to one another. Within the interaction network, 14-3-3 protein ζ/δ is one of the most connected proteins, interacting with HSP90β and tubulin subunits. 14-3-3 protein ζ/δ has been implicated in MT dynamics by regulating tau phosphorylation in bovine brain extracts (84). Interestingly one of the IFN-γ-induced proteins, proteasome activator complex subunit 1 (IGUP I-5111), showed direct tubulin binding within the interactome as well. It will be of interest to study the roles of both 14-3-3 protein ζ/δ and proteasome activator complex subunit 1 in regulating MT dynamics in macrophages.

Of particular interest to this study was the differential recruitment of proteins that may regulate the pronounced MT stabilization in activated macrophages. LPS itself is thought to regulate MT stability and has been shown to bind directly to tubulin *in vitro* (85). However, our MT proteome analysis revealed enhanced association of several stabilizing MAPs with MTs in activated macrophages. We observed enhanced binding of both MAP4 and MAP1S with MTs; both are well known MT wall-binding proteins known to affect MT stabilization (86–88). We also observed enhanced association of CLIP 1 (also called CLIP-170) with MTs that we have shown previously, using cell biology analytical tools, to regulate MT stability in macrophages (5). Our previous IF analysis showed a redistribution of CLIP-170 toward the body of the MT in stabilized MT subsets (5) that with this study includes a quantitative protein enrichment of CLIP-170 on the MT wall. We also saw an increase in EB1 on MTs in activated macrophages (supplemental Table 1). There has been recent interest in the cross-talk between EB1 and CLIP-170 during MT plus (+) end recruitment (50, 89–91), and our study also suggests a potential functional interplay between these proteins during macrophage activation. Interestingly we saw reduced association of stathmin with MTs in IFN-γ/LPS-activated macrophages (supplemental Table 1). Stathmin is a well conserved phosphoprotein that induces MT depolymerization by binding to tubulin dimers and increasing catastrophe rates (92).

We also observed chaperone proteins that consistently copurified with MTs in macrophages. This includes HSP70, which has been reported previously to bind MTs (53, 93) and enhance MT polymerization (53). Of interest to us was HSP90, which has been observed along MTs in mammalian cells (94, 95) and importantly is essential for macrophage activation by LPS (96). In our MT proteomics analysis, we observed a significant increase in HSP90β binding to MTs in macrophages after stimulation by IFN-γ and LPS (supplemental Table 1). Further, treatment of activated macrophages with

the HSP90 antagonist GA strikingly diminished the stability of MTs in these cells. To our knowledge, this is the first time HSP90β has been identified on MTs in macrophages and a potential role for HSP90β in MT stability has been shown. The exact mechanism by which HSP90β regulates MT stability is not clear. One possible explanation is that HSP90β might regulate the activity of stabilizing MAPs via its chaperoning activities. We favor this possibility as recent studies (97, 98) have demonstrated that HSP90β is enriched along acetylated MTs, and chaperones increase the association of tau, an MT-stabilizing protein, with MTs in mouse neurons (98).

Interestingly HSP90 isoforms are essential for proteasome assembly during MHC I antigen presentation (99), and we observed enrichment of several proteasome components along MTs in activated macrophages. HSP90β-generated stabilized MTs may also contribute to the increased vesicular trafficking observed in activated macrophages. Supporting this hypothesis, GA treatment of LPS-activated macrophages causes a marked reduction in cell surface levels of CD14 (100). Further studies will be needed to demonstrate conclusively a role for HSP90β in MT stabilization and function. In summary, deducing the macrophage MAP proteome suggests that there is a complex, multipronged mechanism for MT stabilization in mammalian interphase cells that is coordinated by chaperone proteins, stabilizing MAPs, MT (+) end-binding proteins and catastrophe elements.

Acknowledgment—We thank Sherri Thiele (University of Toronto) for assistance with peritoneal macrophage extraction.

* This work was supported in part by Canadian Institutes of Health Research (CIHR) Grant MOP-68992.

S The on-line version of this article (available at http://www.mcponline.org) contains supplemental Fig. 1 and Table 1.

** Recipient of an Ontario early researcher award and CIHR new investigator award. To whom correspondence should be addressed: Dept. of Cell and Systems Biology, University of Toronto Scarborough, Toronto, Ontario M1C 1A4, Canada. Tel.: 416-287-7377; Fax: 416-287-7676; E-mail: harrison@utsc.utoronto.ca.

REFERENCES

1. Stoppin-Mellet, V., Gaillard, J., and Vantard, M. (2003) Plant katanin, a microtubule severing protein. *Cell Biol. Int.* **27,** 279
2. Mitchison, T., and Kirschner, M. (1984) Dynamic instability of microtubule growth. *Nature* **312,** 237–242
3. Maccioni, R. B., and Cambiazo, V. (1995) Role of microtubule-associated proteins in the control of microtubule assembly. *Physiol. Rev.* **75,** 835–864
4. Mandelkow, E., and Mandelkow, E. M. (1995) Microtubules and microtubule-associated proteins. *Curr. Opin. Cell Biol.* **7,** 72–81
5. Binker, M. G., Zhao, D. Y., Pang, S. J., and Harrison, R. E. (2007) Cytoplasmic linker protein-170 enhances spreading and phagocytosis in activated macrophages by stabilizing microtubules. *J. Immunol.* **179,** 3780–3791
6. Akhmanova, A., Hoogenraad, C. C., Drabek, K., Stepanova, T., Dortland, B., Verkerk, T., Vermeulen, W., Burgering, B. M., De Zeeuw, C. I., Grosveld, F., and Galjart, N. (2001) Clasps are CLIP-115 and -170 associating proteins involved in the regional regulation of microtubule dynamics in motile fibroblasts. *Cell* **104,** 923–935
7. Schuyler, S. C., and Pellman, D. (2001) Microtubule "plus-end-tracking proteins": the end is just the beginning. *Cell* **105,** 421–424
8. Eddé, B., Rossier, J., Le Caer, J. P., Desbruyères, E., Gros, F., and Denoulet, P. (1990) Posttranslational glutamylation of alpha-tubulin. *Science* **247,** 83–85
9. Gundersen, G. G., Kalnoski, M. H., and Bulinski, J. C. (1984) Distinct populations of microtubules: tyrosinated and nontyrosinated alpha tubulin are distributed differently in vivo. *Cell* **38,** 779–789
10. Piperno, G., LeDizet, M., and Chang, X. J. (1987) Microtubules containing acetylated alpha-tubulin in mammalian cells in culture. *J. Cell Biol.* **104,** 289–302
11. Dompierre, J. P., Godin, J. D., Charrin, B. C., Cordelières, F. P., King, S. J., Humbert, S., and Saudou, F. (2007) Histone deacetylase 6 inhibition compensates for the transport deficit in Huntington's disease by increasing tubulin acetylation. *J. Neurosci.* **27,** 3571–3583
12. Reed, N. A., Cai, D., Blasius, T. L., Jih, G. T., Meyhofer, E., Gaertig, J., and Verhey, K. J. (2006) Microtubule acetylation promotes kinesin-1 binding and transport. *Curr. Biol.* **16,** 2166–2172
13. Maiato, H., Sampaio, P., and Sunkel, C. E. (2004) Microtubule-associated proteins and their essential roles during mitosis. *Int. Rev. Cytol.* **241,** 53–153
14. Sedbrook, J. C. (2004) MAPs in plant cells: delineating microtubule growth dynamics and organization. *Curr. Opin. Plant Biol.* **7,** 632–640
15. Morejohn, L. C. (1994) Microtubule binding proteins are not necessarily microtubule-associated proteins. *Plant Cell* **6,** 1696–1699
16. Hamada, T. (2007) Microtubule-associated proteins in higher plants. *J. Plant Res.* **120,** 79–98
17. Liska, A. J., Popov, A. V., Sunyaev, S., Coughlin, P., Habermann, B., Shevchenko, A., Bork, P., Karsenti, E., and Shevchenko, A. (2004) Homology-based functional proteomics by mass spectrometry: application to the Xenopus microtubule-associated proteome. *Proteomics* **4,** 2707–2721
18. Hughes, J. R., Meireles, A. M., Fisher, K. H., Garcia, A., Antrobus, P. R., Wainman, A., Zitzmann, N., Deane, C., Ohkura, H., and Wakefield, J. G. (2008) A microtubule interactome: complexes with roles in cell cycle and mitosis. *PLoS Biol.* **6,** e98
19. O'Connell, P. A., Pinto, D. M., Chisholm, K. A., and MacRae, T. H. (2006) Characterization of the microtubule proteome during post-diapause development of Artemia franciscana. *Biochim. Biophys. Acta* **1764,** 920–928
20. Chuong, S. D., Good, A. G., Taylor, G. J., Freeman, M. C., Moorhead, G. B., and Muench, D. G. (2004) Large-scale identification of tubulin-binding proteins provides insight on subcellular trafficking, metabolic channeling, and signaling in plant cells. *Mol. Cell. Proteomics* **3,** 970–983
21. Sakamoto, T., Uezu, A., Kawauchi, S., Kuramoto, T., Makino, K., Umeda, K., Araki, N., Baba, H., and Nakanishi, H. (2008) Mass spectrometric analysis of microtubule co-sedimented proteins from rat brain. *Genes Cells* **13,** 295–312
22. Nousiainen, M., Silljé, H. H., Sauer, G., Nigg, E. A., and Körner, R. (2006) Phosphoproteome analysis of the human mitotic spindle. *Proc. Natl. Acad. Sci. U.S.A.* **103,** 5391–5396
23. Sauer, G., Körner, R., Hanisch, A., Ries, A., Nigg, E. A., and Silljé, H. H. (2005) Proteome analysis of the human mitotic spindle. *Mol. Cell. Proteomics* **4,** 35–43
24. Mack, G. J., and Compton, D. A. (2001) Analysis of mitotic microtubule-associated proteins using mass spectrometry identifies astrin, a spindle-associated protein. *Proc. Natl. Acad. Sci. U.S.A.* **98,** 14434–14439
25. Reinders, Y., Schulz, I., Gräf, R., and Sickmann, A. (2006) Identification of novel centrosomal proteins in Dictyostelium discoideum by comparative proteomic approaches. *J. Proteome Res.* **5,** 589–598
26. Andersen, J. S., Wilkinson, C. J., Mayor, T., Mortensen, P., Nigg, E. A., and Mann, M. (2003) Proteomic characterization of the human centrosome by protein correlation profiling. *Nature* **426,** 570–574
27. Inglis, P. N., Boroevich, K. A., and Leroux, M. R. (2006) Piecing together a ciliome. *Trends Genet.* **22,** 491–500
28. Pazour, G. J., Agrin, N., Leszyk, J., and Witman, G. B. (2005) Proteomic analysis of a eukaryotic cilium. *J. Cell Biol.* **170,** 103–113
29. Dinarello, C. A. (1996) Biologic basis for interleukin-1 in disease. *Blood* **87,** 2095–2147
30. Akira, S., Taga, T., and Kishimoto, T. (1993) Interleukin-6 in biology and medicine. *Adv. Immunol.* **54,** 1–78
31. Tracey, K. J., and Cerami, A. (1994) Tumor necrosis factor: a pleiotropic

cytokine and therapeutic target. *Annu. Rev. Med.* **45,** 491–503
32. Schroder, K., Hertzog, P. J., Ravasi, T., and Hume, D. A. (2004) Interferon-gamma: an overview of signals, mechanisms and functions. *J. Leukoc. Biol.* **75,** 163–189
33. Cross, A. S., Sadoff, J. C., Kelly, N., Bernton, E., and Gemski, P. (1989) Pretreatment with recombinant murine tumor necrosis factor alpha/cachectin and murine interleukin 1 alpha protects mice from lethal bacterial infection. *J. Exp. Med.* **169,** 2021–2027
34. Allen, J. N., Moore, S. A., Liao, Z., and Wewers, M. D. (1997) Changes in mononuclear phagocyte microtubules after endotoxin stimulation. I. Changes in microtubule stability. *Am. J. Respir. Cell Mol. Biol.* **16,** 119–126
35. Schroer, T. A., Steuer, E. R., and Sheetz, M. P. (1989) Cytoplasmic dynein is a minus end-directed motor for membranous organelles. *Cell* **56,** 937–946
36. Vallee, R. B. (1982) A Taxol-dependent procedure for the isolation of microtubules and microtubule-associated proteins (MAPs). *J. Cell Biol.* **92,** 435–442
37. Zhang, B., VerBerkmoes, N. C., Langston, M. A., Uberbacher, E., Hettich, R. L., and Samatova, N. F. (2006) Detecting differential and correlated protein expression in label-free shotgun proteomics. *J. Proteome Res.* **5,** 2909–2918
38. Old, W. M., Meyer-Arendt, K., Aveline-Wolf, L., Pierce, K. G., Mendoza, A., Sevinsky, J. R., Resing, K. A., and Ahn, N. G. (2005) Comparison of label-free methods for quantifying human proteins by shotgun proteomics. *Mol. Cell. Proteomics* **4,** 1487–1502
39. Khandani, A., Eng, E., Jongstra-Bilen, J., Schreiber, A. D., Douda, D., Samavarchi-Tehrani, P., and Harrison, R. E. (2007) Microtubules regulate PI-3K activity and recruitment to the phagocytic cup during Fc-gamma receptor-mediated phagocytosis in nonelicited macrophages. *J. Leukoc. Biol.* **82,** 417–428
40. Bajno, L., Peng, X. R., Schreiber, A. D., Moore, H. P., Trimble, W. S., and Grinstein, S. (2000) Focal exocytosis of VAMP3-containing vesicles at sites of phagosome formation. *J. Cell Biol.* **149,** 697–706
41. Ashburner, M., Ball, C. A., Blake, J. A., Botstein, D., Butler, H., Cherry, J. M., Davis, A. P., Dolinski, K., Dwight, S. S., Eppig, J. T., Harris, M. A., Hill, D. P., Issel-Tarver, L., Kasarskis, A., Lewis, S., Matese, J. C., Richardson, J. E., Ringwald, M., Rubin, G. M., and Sherlock, G. (2000) Gene ontology: tool for the unification of biology. The Gene Ontology Consortium. *Nat. Genet.* **25,** 25–29
42. Breitkreutz, B. J., Stark, C., and Tyers, M. (2003) Osprey: a network visualization system. *Genome Biol.* **4,** R22
43. Westermann, S., and Weber, K. (2003) Post-translational modifications regulate microtubule function. *Nat. Rev. Mol. Cell Biol.* **4,** 938–947
44. Sakurai, T., Fujita, Y., Ohto, E., Oguro, A., and Atomi, Y. (2005) The decrease of the cytoskeleton tubulin follows the decrease of the associating molecular chaperone alphaB-crystallin in unloaded soleus muscle atrophy without stretch. *FASEB J.* **19,** 1199–1201
45. Fujita, Y., Ohto, E., Katayama, E., and Atomi, Y. (2004) alphaB-Crystallin-coated MAP microtubule resists nocodazole and calcium-induced disassembly. *J. Cell Sci.* **117,** 1719–1726
46. von Massow, A., Mandelkow, E. M., and Mandelkow, E. (1989) Interaction between kinesin, microtubules, and microtubule-associated protein 2. *Cell. Motil. Cytoskeleton* **14,** 562–571
47. Lye, R. J., Porter, M. E., Scholey, J. M., and McIntosh, J. R. (1987) Identification of a microtubule-based cytoplasmic motor in the nematode C. elegans. *Cell* **51,** 309–318
48. Wilde, A., Lizarraga, S. B., Zhang, L., Wiese, C., Gliksman, N. R., Walczak, C. E., and Zheng, Y. (2001) Ran stimulates spindle assembly by altering microtubule dynamics and the balance of motor activities. *Nat. Cell Biol.* **3,** 221–227
49. Zou, T., Ouyang, L., Chen, L., Dong, W., Qiao, H., Liu, Y., and Qi, Y. (2008) The role of microtubule-associated protein 1S in SOCS3 regulation of IL-6 signaling. *FEBS Lett.* **582,** 4015–4022
50. Tirnauer, J. S., Grego, S., Salmon, E. D., and Mitchison, T. J. (2002) EB1-microtubule interactions in Xenopus egg extracts: role of EB1 in microtubule stabilization and mechanisms of targeting to microtubules. *Mol. Biol. Cell* **13,** 3614–3626
51. Nguyen, H. L., Gruber, D., McGraw, T., Sheetz, M. P., and Bulinski, J. C. (1998) Stabilization and functional modulation of microtubules by microtubule-associated protein 4. *Biol. Bull.* **194,** 354–357
52. Garnier, C., Barbier, P., Gilli, R., Lopez, C., Peyrot, V., and Briand, C. (1998) Heat-shock protein 90 (hsp90) binds in vitro to tubulin dimer and inhibits microtubule formation. *Biochem. Biophys. Res. Commun.* **250,** 414–419
53. Williams, N. E., and Nelsen, E. M. (1997) HSP70 and HSP90 homologs are associated with tubulin in hetero-oligomeric complexes, cilia and the cortex of Tetrahymena. *J. Cell Sci.* **110,** 1665–1672
54. Gordon, M. A., Jack, D. L., Dockrell, D. H., Lee, M. E., and Read, R. C. (2005) Gamma interferon enhances internalization and early nonoxidative killing of Salmonella enterica serovar Typhimurium by human macrophages and modifies cytokine responses. *Infect. Immun.* **73,** 3445–3452
55. Nacife, V. P., Soeiro Mde, N., Gomes, R. N., D'Avila, H., Castro-Faria Neto, H. C., and Meirelles Mde, N. (2004) Morphological and biochemical characterization of macrophages activated by carrageenan and lipopolysaccharide in vivo. *Cell Struct. Funct.* **29,** 27–34
56. Janský, L., Reymanová, P., and Kopecký, J. (2003) Dynamics of cytokine production in human peripheral blood mononuclear cells stimulated by LPS or infected by Borrelia. *Physiol. Res.* **52,** 593–598
57. Schmidt, A., Caron, E., and Hall, A. (2001) Lipopolysaccharide-induced activation of beta2-integrin function in macrophages requires Irak kinase activity, p38 mitogen-activated protein kinase, and the Rap1 GTPase. *Mol. Cell. Biol.* **21,** 438–448
58. Spinelle-Jaegle, S., Devillier, P., Doucet, S., Millet, S., Banissi, C., Diu-Hercend, A., and Ruuth, E. (2001) Inflammatory cytokine production in interferon-gamma-primed mice, challenged with lipopolysaccharide. Inhibition by SK&F 86002 and interleukin-1 beta-converting enzyme inhibitor. *Eur. Cytokine Netw.* **12,** 280–289
59. Hermann, P., Rubio, M., Nakajima, T., Delespesse, G., and Sarfati, M. (1998) IFN-alpha priming of human monocytes differentially regulates gram-positive and gram-negative bacteria-induced IL-10 release and selectively enhances IL-12p70, CD80, and MHC class I expression. *J. Immunol.* **161,** 2011–2018
60. Meda, L., Gasperini, S., Ceska, M., and Cassatella, M. A. (1994) Modulation of proinflammatory cytokine release from human polymorphonuclear leukocytes by gamma interferon. *Cell. Immunol.* **157,** 448–461
61. Xie, B., Dong, Z., and Fidler, I. J. (1994) Regulatory mechanisms for the expression of type IV collagenases/gelatinases in murine macrophages. *J. Immunol.* **152,** 3637–3644
62. Nash, T. W., Libby, D. M., and Horwitz, M. A. (1988) IFN-gamma-activated human alveolar macrophages inhibit the intracellular multiplication of Legionella pneumophila. *J. Immunol.* **140,** 3978–3981
63. Wirth, J. J., Kierszenbaum, F., Sonnenfeld, G., and Zlotnik, A. (1985) Enhancing effects of gamma interferon on phagocytic cell association with and killing of Trypanosoma cruzi. *Infect. Immun.* **49,** 61–66
64. Cooper, P. H., Mayer, P., and Baggiolini, M. (1984) Stimulation of phagocytosis in bone marrow-derived mouse macrophages by bacterial lipopolysaccharide: correlation with biochemical and functional parameters. *J. Immunol.* **133,** 913–922
65. Valiron, O., Caudron, N., and Job, D. (2001) Microtubule dynamics. *Cell. Mol. Life Sci.* **58,** 2069–2084
66. Gundersen, G. G., and Cook, T. A. (1999) Microtubules and signal transduction. *Curr. Opin. Cell Biol.* **11,** 81–94
67. Nabi, I. R. (1999) The polarization of the motile cell. *J. Cell Sci.* **112,** 1803–1811
68. Walker, P. R., and Whitfield, J. F. (1985) Cytoplasmic microtubules are essential for the formation of membrane-bound polyribosomes. *J. Biol. Chem.* **260,** 765–770
69. Wickham, L., Duchaîne, T., Luo, M., Nabi, I. R., and DesGroseillers, L. (1999) Mammalian staufen is a double-stranded-RNA- and tubulin-binding protein which localizes to the rough endoplasmic reticulum. *Mol. Cell. Biol.* **19,** 2220–2230
70. Hovland, R., Hesketh, J. E., and Pryme, I. F. (1996) The compartmentalization of protein synthesis: importance of cytoskeleton and role in mRNA targeting. *Int. J. Biochem. Cell Biol.* **28,** 1089–1105
71. Litman, P., Barg, J., and Ginzburg, I. (1994) Microtubules are involved in the localization of tau mRNA in primary neuronal cell cultures. *Neuron* **13,** 1463–1474
72. Groettrup, M., Soza, A., Eggers, M., Kuehn, L., Dick, T. P., Schild, H., Rammensee, H. G., Koszinowski, U. H., and Kloetzel, P. M. (1996) A role for the proteasome regulator PA28alpha in antigen presentation. *Nature*

381, 166–168
73. Groettrup, M., Ruppert, T., Kuehn, L., Seeger, M., Standera, S., Koszinowski, U., and Kloetzel, P. M. (1995) The interferon-gamma-inducible 11 S regulator (PA28) and the LMP2/LMP7 subunits govern the peptide production by the 20 S proteasome in vitro. *J. Biol. Chem.* **270,** 23808–23815
74. Realini, C., Dubiel, W., Pratt, G., Ferrell, K., and Rechsteiner, M. (1994) Molecular cloning and expression of a gamma-interferon-inducible activator of the multicatalytic protease. *J. Biol. Chem.* **269,** 20727–20732
75. Frentzel, S., Kuhn-Hartmann, I., Gernold, M., Gött, P., Seelig, A., and Kloetzel, P. M. (1993) The major-histocompatibility-complex-encoded beta-type proteasome subunits LMP2 and LMP7. Evidence that LMP2 and LMP7 are synthesized as proproteins and that cellular levels of both mRNA and LMP-containing 20S proteasomes are differentially regulated. *Eur. J. Biochem.* **216,** 119–126
76. Noble, M., Lewis, S. A., and Cowan, N. J. (1989) The microtubule binding domain of microtubule-associated protein MAP1B contains a repeated sequence motif unrelated to that of MAP2 and tau. *J. Cell Biol.* **109,** 3367–3376
77. Chen, H. J., Lin, C. M., Lin, C. S., Perez-Olle, R., Leung, C. L., and Liem, R. K. (2006) The role of microtubule actin cross-linking factor 1 (MACF1) in the Wnt signaling pathway. *Genes Dev.* **20,** 1933–1945
78. Lewkowicz, E., Herit, F., Le Clainche, C., Bourdoncle, P., Perez, F., and Niedergang, F. (2008) The microtubule-binding protein CLIP-170 coordinates mDia1 and actin reorganization during CR3-mediated phagocytosis. *J. Cell Biol.* **183,** 1287–1298
79. Patel, P. C., and Harrison, R. E. (2008) Membrane ruffles capture C3bi-opsonized particles in activated macrophages. *Mol. Biol. Cell* **19,** 4628–4639
80. Paddison, P. J., Caudy, A. A., Bernstein, E., Hannon, G. J., and Conklin, D. S. (2002) Short hairpin RNAs (shRNAs) induce sequence-specific silencing in mammalian cells. *Genes Dev.* **16,** 948–958
81. Peachman, K. K., Rao, M., Palmer, D. R., Zidanic, M., Sun, W., Alving, C. R., and Rothwell, S. W. (2004) Functional microtubules are required for antigen processing by macrophages and dendritic cells. *Immunol. Lett.* **95,** 13–24
82. Song, E., Ouyang, N., Hörbelt, M., Antus, B., Wang, M., and Exton, M. S. (2000) Influence of alternatively and classically activated macrophages on fibrogenic activities of human fibroblasts. *Cell. Immunol.* **204,** 19–28
83. Goerdt, S., Politz, O., Schledzewski, K., Birk, R., Gratchev, A., Guillot, P., Hakiy, N., Klemke, C. D., Dippel, E., Kodelja, V., and Orfanos, C. E. (1999) Alternative versus classical activation of macrophages. *Pathobiology* **67,** 222–226
84. Agarwal-Mawal, A., Qureshi, H. Y., Cafferty, P. W., Yuan, Z., Han, D., Lin, R., and Paudel, H. K. (2003) 14-3-3 connects glycogen synthase kinase-3 beta to tau within a brain microtubule-associated tau phosphorylation complex. *J. Biol. Chem.* **278,** 12722–12728
85. Risco, C., Domínguez, J. E., Bosch, M. A., and Carrascosa, J. L. (1993) Biochemical and electron microscopy analysis of the endotoxin binding to microtubules in vitro. *Mol. Cell. Biochem.* **121,** 67–74
86. Murphy, D. B., Johnson, K. A., and Borisy, G. G. (1977) Role of tubulin-associated proteins in microtubule nucleation and elongation. *J. Mol. Biol.* **117,** 33–52
87. Borisy, G. G., Marcum, J. M., Olmsted, J. B., Murphy, D. B., and Johnson, K. A. (1975) Purification of tubulin and associated high molecular weight proteins from porcine brain and characterization of microtubule assembly in vitro. *Ann. N.Y. Acad. Sci.* **253,** 107–132
88. Weingarten, M. D., Lockwood, A. H., Hwo, S. Y., and Kirschner, M. W. (1975) A protein factor essential for microtubule assembly. *Proc. Natl. Acad. Sci. U.S.A.* **72,** 1858–1862
89. Manna, T., Honnappa, S., Steinmetz, M. O., and Wilson, L. (2008) Suppression of microtubule dynamic instability by the +TIP protein EB1 and its modulation by the CAP-Gly domain of p150glued. *Biochemistry* **47,** 779–786
90. Ligon, L. A., Shelly, S. S., Tokito, M. K., and Holzbaur, E. L. (2006) Microtubule binding proteins CLIP-170, EB1, and p150Glued form distinct plus-end complexes. *FEBS Lett.* **580,** 1327–1332
91. Mimori-Kiyosue, Y., Grigoriev, I., Lansbergen, G., Sasaki, H., Matsui, C., Severin, F., Galjart, N., Grosveld, F., Vorobjev, I., Tsukita, S., and Akhmanova, A. (2005) CLASP1 and CLASP2 bind to EB1 and regulate microtubule plus-end dynamics at the cell cortex. *J. Cell Biol.* **168,** 141–153
92. Belmont, L. D., and Mitchison, T. J. (1996) Identification of a protein that interacts with tubulin dimers and increases the catastrophe rate of microtubules. *Cell* **84,** 623–631
93. Clark, B. D., and Brown, I. R. (1987) Altered expression of a heat shock protein in the mammalian nervous system in the presence of agents which affect microtubule stability. *Neurochem. Res.* **12,** 819–823
94. Czar, M. J., Welsh, M. J., and Pratt, W. B. (1996) Immunofluorescence localization of the 90-kDa heat-shock protein to cytoskeleton. *Eur. J. Cell Biol.* **70,** 322–330
95. Redmond, T., Sanchez, E. R., Bresnick, E. H., Schlesinger, M. J., Toft, D. O., Pratt, W. B., and Welsh, M. J. (1989) Immunofluorescence colocalization of the 90-kDa heat-shock protein and microtubules in interphase and mitotic mammalian cells. *Eur. J. Cell Biol.* **50,** 66–75
96. Byrd, C. A., Bornmann, W., Erdjument-Bromage, H., Tempst, P., Pavletich, N., Rosen, N., Nathan, C. F., and Ding, A. (1999) Heat shock protein 90 mediates macrophage activation by Taxol and bacterial lipopolysaccharide. *Proc. Natl. Acad. Sci. U.S.A.* **96,** 5645–5650
97. Giustiniani, J., Daire, V., Cantaloube, I., Durand, G., Poüs, C., Perdiz, D., and Baillet, A. (2009) Tubulin acetylation favors Hsp90 recruitment to microtubules and stimulates the signaling function of the Hsp90 clients Akt/PKB and p53. *Cell. Signal.* **21,** 529–539
98. Dou, F., Netzer, W. J., Tanemura, K., Li, F., Hartl, F. U., Takashima, A., Gouras, G. K., Greengard, P., and Xu, H. (2003) Chaperones increase association of tau protein with microtubules. *Proc. Natl. Acad. Sci. U.S.A.* **100,** 721–726
99. Yamano, T., Mizukami, S., Murata, S., Chiba, T., Tanaka, K., and Udono, H. (2008) Hsp90-mediated assembly of the 26 S proteasome is involved in major histocompatibility complex class I antigen processing. *J. Biol. Chem.* **283,** 28060–28065
100. Vega, V. L., and De Maio, A. (2003) Geldanamycin treatment ameliorates the response to LPS in murine macrophages by decreasing CD14 surface expression. *Mol. Biol. Cell* **14,** 764–773